

Contents lists available at ScienceDirect

Engineering Science and Technology, an International Journal

journal homepage: www.elsevier.com/locate/jestch



Nanofluids stability on amino-silane and polymers coating titanium dioxide and zinc oxide nanoparticles



Anis Arisa Roslan a,*, Siti Nur Azella Zaine , Hasnah Mohd Zaid , Mursyidah Umar b, Hoe Guan Beh

^a Fundamental & Applied Science Department, Centre of Innovative Nanostructure & Nanodevices (COINN), Universiti Teknologi PETRONAS, Seri Iskandar, Perak 32610, Malaysia ^b Department of Petroleum Engineering, Universitas Islam Riau, Pekanbaru, Riau 28284, Indonesia

ARTICLE INFO

Article history: Received 20 January 2022 Revised 6 September 2022 Accepted 2 December 2022 Available online 27 December 2022

Keywords: Nanofluids Titanium dioxide Zinc oxide Stability Surface coating

ABSTRACT

The nanofluids technology keeps advancing in the recent decades despite the modus operandi in formulating stable nanofluids is still in the grey area. This paper provides a further understanding of the nanoparticles and nanofluids synthesis methods with surface modification alternative in contemplation of nanofluid stability enhancement. Due to the shortcomings of this technology, which is the dispersity and stability issue owing to the van Der Waals attraction, this paper reports a full formulation design guideline in term of the temperature, crystal growth duration, nanoparticles concentration, pH and nanofluids synthesis method to obtain the stable titanium dioxide (TiO2) and zinc oxide (ZnO) nanofluids. Compatibility of polymers polyethylene glycol (PEG), polyvinyl alcohol (PVA), polyvinylpyrrolidone (PVP) and an amino-silane; (3-Aminopropyl) triethoxysilane (APTES) with the synthesized nanoparticles were observed. Our findings discovered that the compatible polymer-nanoparticle composites are TiO2-PVP and ZnO-PEG with zeta potential values at 47.2 mV and 56.5 mV respectively.

© 2022 Karabuk University. Publishing services by Elsevier B.V. This is an open access article under the CC BY-NC-ND license (http://creativecommons.org/licenses/by-nc-nd/4.0/).

1. Introduction

In recent years, numerous studies have looked into nanofluids for many different types of systems and technologies. Nanofluids have various and particular functions in stable colloidal suspension form. For enhanced oil recovery (EOR) application, nanofluids can be the solutions for numerous problems because of their outstanding features and properties. Nanofluids have the ability to pass through the channels and flow smoothly in order to employ the heat transfer [1] because of their large surface area, as compared to the conventional fluids that have large agglomeration and clogged in the small passages.

In the oil and gas field, nanofluids are the most preferred method other than surfactant flooding and polymer flooding [2]. The ultimate function of nanofluids in enhanced oil recovery application is from the interaction of the fluid with rock/oil system [3]. The ultra-small size of nanoparticles managed them to penetrate and flow through the pores where the traditional macro or micro particle-size fluids unable to pass through. Hence, nanoparticles are able to have more contact swept zones and improve the injection fluids efficiency to extract more oil from the reservoir [4]. A

E-mail address: anis.roslan.22@ucl.ac.uk (A.A. Roslan). Peer review under responsibility of Karabuk University. reported study mentioned that the factor of oil recovery increases up to 30 % when miscible nanofluids were applied for the water injection [5]. On the other hand, for the case of nanoparticles that were immiscible with base fluids, the factor of oil recovery solely increased up to 20 %. The findings deduced that the success rate of oil recovery with the application of immiscible nanofluids are slightly lower than that of miscible nanofluids.

Based on the rapid evolution of nanotechnology, metal oxides have been the interest for nanofluid application. There is a characteristic that exists in metal oxides to obtain charge separation capacity which distinguishes them from other metals. Certain oxides nanoparticles can disperse freely into polar base-fluids and experience a phenomenon called the dispersible process [6]. This study focusses on titanium dioxide (TiO₂) and zinc oxide (ZnO) nanoparticles because of their unique electronic characteristic and wide band gap energy which give large exciton binding energy [7]. In spite of that, stability issue is still has been one of the difficulties during the fabrication [8].

It is known that the stability of the suspension is very important for nanofluids, especially in extending the duration of usage. Aggregation and deposition are the two main challenges of nanofluids stability [9]. Most reported studies encountered problems of unstable chemical, thermal and rheological properties at High Pressure/High Temperature (HPHT) condition when polymer additives were used [10,11] especially in drilling or downhole pro-

^{*} Corresponding author.

cesses [12]. The statement is contradicted with some literatures that mentioned the behavior of nanoparticles/polymer was found stable, especially the rheological properties in HPHT conditions [13]. It is supported by other study that the application of nanoparticles in the fluids gives stability and improve the mentioned properties at pressure and temperature up to 272 MPa and 300 °C respectively [14].

The state-of-the-art research on nanofluids are mainly on creating hybrid, polymer blended nanocomposites because of the characteristics of the formulated nanofluids for their appropriate applications. For instance, the formulated Ce-doped TiO₂/poly(nbutyl methacrylate) nanocomposites for electrical applications [15], polymer/silver-zinc oxide nanocomposite for gas sensor applications [7], zinc oxide-multiwalled carbon nanotube nanocomposites for engine oil lubrication [16] and single-walled carbon nanotubes nanofluid for heat transfer in refrigeration system [17]. However, the preparation procedure in achieving stable nanofluids has not been emphasized and the methodology has not been thoroughly explained. Since the main obstacles to conducting research using nanofluids are high expenses [18], this paper demonstrates on the synthesis method to creating stable nanofluids. The preparation process of the nanoparticles will significantly affect the characteristics and performance of nanofluids. Hence, the preparation step of nanoparticles and nanofluids need to be highlighted as it is very crucial [19]. There are many aspects that need to be considered during the synthetization such as temperature, nanoparticle size [20], volume fraction and shape of nanoparticles [21] as design parameters.

Polymer coating could be the solution to improve the stability and surface properties of nanoparticles for EOR [22], but still needs thorough investigation and studies specifically for HPHT conditions. The polymeric component in the base fluid is said to give better distribution of nanoparticles throughout the drilling fluid composition. Nevertheless, the compatibility between the blended polymer and nanocomposites might become one of the drawbacks [7]. Water-soluble polymers have become the option to be the base fluid for nanoparticles, such as polyacrylamide. It is reported that nanoparticles dispersed in polyacrylamide is stable for a significant time [23]. Research has found that ethylene glycol (EG) based NFs that contained oxides has superior features with the highest thermal conductivity and lowest viscosity [2]. Other than that, polymer polyvinylpyrrolidone (PVP) is used as the base fluid and to further improve the dispersion of nanoparticles/polymer, surfactant has also been applied [24]. A published literature has reported that high density, low molecular weight with thermally stable monomer is the type of polymeric solution that can withstand HPHT environment. Emulsifiers or modifiers with fatty acids, fatty alcohols, silanes and amines functional groups, including polymers [25] were mentioned to be used at up to 248 °C [26]. The polymer-treated nanoparticles were expected to have more stable network by the bridging of the polymers among nanoparticles since the adsorption of the polymers from attached sites is irreversible and not easily broken.

2. Methodology

The experimental methods consist of the preparation of brine solution, synthesis of non-modified and modified titanium dioxide and zinc oxide nanoparticles. The synthesized nanoparticles were dried into powder form for XRD, FTIR, FESEM and TEM characterizations.

On the other hand, using the prepared brine solution, nanofluids were formulated by one-step method; skipping the drying process. The stability of nanofluids was analyzed from physical observation and zeta potential measurements.

2.1. Chemicals and materials used

The chemicals used to synthesis TiO₂ nanoparticles are acetic acid and nitric acid and titanium (IV) isopropoxide (TTIP). Meanwhile, the chemical needed for the synthesis of ZnO nanoparticles is zinc acetate dihydrate. Both TiO₂ and ZnO nanoparticles synthesis require sodium hydroxide (NaOH) solution, Teflon lined hydrothermal autoclave comprises stainless steel (SS-316) and polytetrafluoroethylene (PTFE) were used. For the surface modification of the nanoparticles, the chemicals used are three different polymers; polyethene glycol (PEG), poly (vinyl alcohol) (PVA), polyvinylpyrrolidone (PVP) and an amino silane; 3-aminopropyl) triethoxysilane (APTES). To produce nanofluids, sodium chloride (NaCl) is needed to formulate brine solution as the continuous phase. All of the chemicals were purchased from Sigma Aldrich (M) Sdn. Bhd. and Merck & Co., Inc. A&D Weighing GR-202 analytical balance was used for all the weight measurements done in this study with precision of up to 0.0001 g.

2.2. Synthesis of TiO₂ nanoparticles and surface modification

The samples were synthesized via hydrothermal method at growth time and temperature. The hydrothermal reactor pressure is at 3 MPa (30 bar) at the rate of 5 °C/minute. This synthesis method is chosen to be a favourable synthesis method because it needs simple equipment, low in cost, easy to handle and environmental-friendly [27,28]. Hydrothermal synthesis method acquires technique of growing crystal from high temperature aqueous solutions at high vapor pressure in the steel pressure vessel called autoclave, where the nutrient solutes supplied along with water for the crystal growth. Crystallization occurred due to the combination of reaction conditions which are inorganic cations; OH⁻ and the ratio of nanoparticles precursors. Crystallization rate is directly proportional to temperature while nucleation rate is inversely proportional to temperature [29]. From previous studies, the hydrothermal growth time and temperature set by other researchers were different for all of the nanoparticles, according to the desired morphology and crystal habits on the synthesized nanoparticles. As for ZnO nanoparticles, the temperature ranged at 60 to 200 °C with growth time ranged from 2 to 12 h [30–32]. The hydrothermal temperature for TiO₂ nanoparticles were done at the range of 80 to 250 °C with growth time ranged from 6 to 24 h [16,33,34,35].

2.3. Preparation of brine solution

NaCl was measured for 0.002 molL⁻¹ of brine solution to mimic the salinity of sea water for the brine solution formulation. The distilled water as the solvent for brine solution was prepared from Water Still-WS 4L.

2.4. Synthesis of TiO₂ nanoparticles

In synthesizing TiO₂ nanoparticles, the hydrolysis process was done by using 0.2 M of TTIP and 0.2 M of acetic acid. The solution was mixed and stirred at room temperature for 15 min. Then, 290 ml of deionized water was added and stirred for 1 h at 700 rpm. 4 ml of nitric acid was then added and stirred for 2 h at 80 °C for the complete peptization process before another 370 ml of deionized water was added. Then, the solution mixture was transferred into Teflon lined stainless-steel autoclave for the hydrothermal growth process. The process was proceeding with growth time at 12 h and temperature at 120 °C. Later, 2.4 ml of nitric acid was added dropwise, and the precipitate was sonicated using an ultrasonic horn at 80 % amplitude, 15 times for 1 min.

Before sample characterization, the three samples produced were washed with ethanol.

2.5. Synthesis of ZnO nanoparticles

In the synthesis of ZnO, two different solutions were prepared. The first solution containing 1 M of zinc acetate dihydrate (ZnC $_4$ H $_6$ O $_4$) in 100 ml of deionized water. The second solution containing 1 M of sodium hydroxide (NaOH) in 100 ml of deionized water. The NaOH solution was added into the ZnC $_4$ H $_6$ O $_4$ solution, dropwisely. The mixture was then stirred at 600 rpm at room temperature for 15 min. The solution mixture was then transferred into Teflon lined stainless-steel autoclave for hydrothermal growth process at a different time and temperature; 2 h at 100 °C, 6 h at 60 °C and 12 h at 150 °C. The three samples of ZnO nanoparticles produced at three different synthesis parameters were washed with ethanol prior to characterization.

2.6. Surface modification of nanoparticles

Three different polymers; polyethene glycol (PEG), poly (vinyl alcohol) (PVA), polyvinylpyrrolidone (PVP) and an amino silane; 3-aminopropyl) triethoxysilane (APTES) were used to coat the surface of TiO₂ and ZnO nanoparticles respectively. In the experiment, 0.3 wt% of the polymers and amino silane solutions were by using deionized water as the solvent. The solution was then mixed with the synthesized nanoparticles. The mixture of the nanoparticles and polymer were stirred continuously at 50 °C for two days. The excess solvent was then separated using a vacuum filter system.

2.7. Preparation of nanofluids

The nanofluids were prepared by one-step method with 0.25 wt % of nanoparticles dispersed in 10 ml of brine as the base fluid. During washing, it was centrifuged with ethanol 3 times and with brine solution during the fourth time.

2.8. Characterizations

The physicochemical properties of the synthesized TiO₂ and ZnO nanoparticles were characterized by advanced analytical equipment such as Fourier-Transform Infrared (FTIR); Thermo Scientific Nicolet iS50, X-ray Diffraction (XRD); Bruker AXS D8, Field Emission Scanning Electron Microscopy (FESEM); Ziess Supra 55 VP, Transmission Electron Microscope (TEM); Zeiss Libra 200FE and zeta potential; Malvern Master Sizer 2000.

3. Results and discussion

The results obtained are presented and discussed in this section.

3.1. XRD results

The synthesized nanoparticles were characterized by XRD, model Bruker AXS D8, for their phase peaks identification. The X-ray diffraction patterns of the synthesized non-modified and modified TiO₂ nanoparticles are shown in Fig. 1. The obtained diffraction patterns matched with the datasheet JCPDS: 894921. The peaks at 25.32°, 37.13°, 37.90°, 38.80°, 48.22°, 54.10°, 55.23°, 62.92, 69.05°, 70.56° and 75.45° correspond of 2θ peaks corresponded to the (101), (103), (004), (112), (200), (105), (211), (204), (116), (220) and (215) crystalline planes of anatase TiO₂ structure. All the diffraction peaks for the surface modified TiO₂ show well indexed to purely anatase phase. No characteristic peaks were detected for the rutile phase, brookite phase, or any other

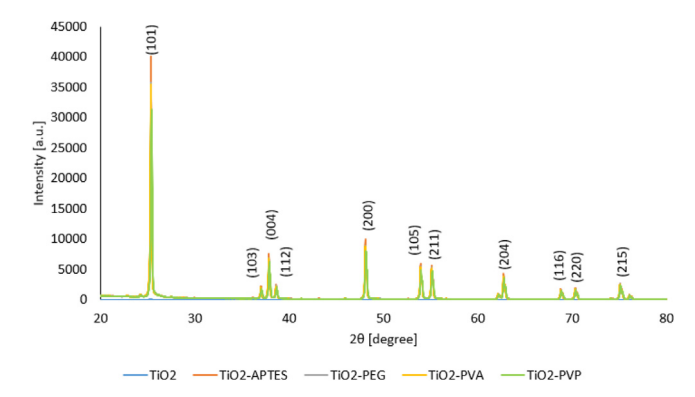


Fig. 1. XRD graph on TiO₂ and surface-modified TiO₂ nanoparticles.

impurities. Unlike other nanoparticles in this study, TiO₂ showed no effect on the main planes with regard to the coating. From the calculated values, the crystallite size of TiO₂ nanoparticles is bigger as compared to other nanoparticles in this study. This show that the synthesized TiO₂ nanoparticles are coated mechanically with the coatings, not chemically or covalently bonded, as the XRD peaks showed no distortions from any secondary reactions or overlapping peaks.

The sharpness of the peaks shows that the nanoparticles are highly crystalline. The XRD tests on the modified TiO_2 nanoparticles are found to be identical to the unmodified TiO_2 nanoparticles. From the XRD patterns, the silane group and the polymers give no impact on the crystal structure of the TiO_2 nanoparticles. The crystallite size of the anatase TiO_2 at (101) plane was calculated by on Scherer equation and the result was tabulated in Table 1.

From the plotted XRD graphs, the crystallite size was calculated using the Scherrer equation as shown in Equation (1), where D is the crystallite size, κ is the Scherrer constant at 0.9, λ is the wavelength of X-ray source value at 0.15406 nm, β is the full width at half minimum (FWHM) and θ is the Bragg angle of the plane. The FWHM values were obtained using software that performs a Gaussian fit from the plotted graphs which is OriginPro 9.0.

$$D = \frac{\kappa \lambda}{\beta COS\theta} \tag{1}$$

The results show that pure TiO₂, TiO₂-APTES, TiO₂-PEG, TiO₂-PVA and TiO₂-PVP exhibit crystallite sizes of 31.39 nm, 51.08 nm, 50.17 nm, 49.26 nm and 47.91 nm, respectively. Based on the calculated results, even though surface modification by using polymers and amino silane does not affect the crystallinity of the synthesized nanoparticles, yet the surface modification does affect the crystallite sizes. The surface modification has increased in the crystallite size of the modified TiO₂ nanoparticles.

Fig. 2 shows the XRD patterns of the synthesized ZnO, ZnO-APTES, ZnO-PEG, ZnO-PVA and ZnO-PVP. The spectra of the diffraction peaks confirmed the crystallinity of the synthesized nanoparticles. The peaks at 31.80°, 34.45°, 36.21°, 47.65°, 56.72°, 62.95°, 66.60°, 68.10°, 69.40°, 71.92° and 77.30° of 20 were assigned at the (100), (002), (101), (102), (110), (103), (200), (112),

Table 1
Calculated XRD characteristics for non-modified and modified TiO₂

Nanoparticle	FWHM (rad)	2θ (°)	D (nm)
TiO ₂ TiO ₂ -APTES	0.27100 0.16657	25.26524 25.34402	31.39
TiO ₂ -APTES TiO ₂ -PEG	0.16959	25.34402 25.34402	51.08 50.17
TiO ₂ -PVA	0.17269	25.31776 25.31776	49.26
TiO ₂ -PVP	0.17759	25.31776	47.91

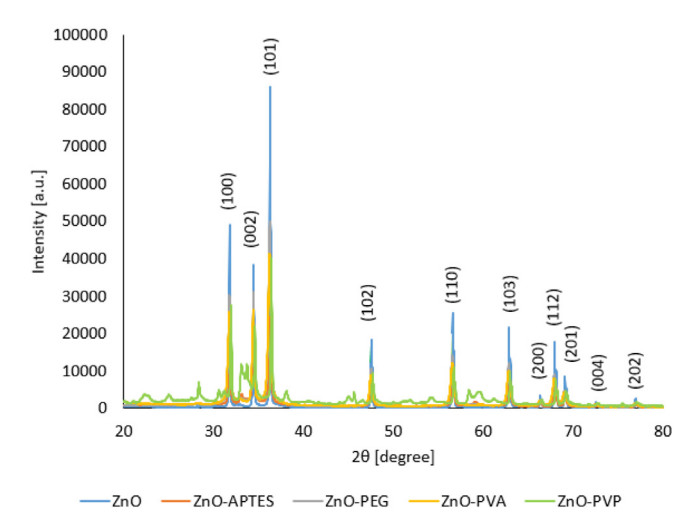


Fig. 2. XRD graph on ZnO and surface-modified ZnO nanoparticles.

(201), (004) and (202) planes of ZnO nanoparticles which matched with datasheet JCPDS:36–1451. The crystallite size of the synthesized samples was calculated by using the Scherer equation of the most intense peak of (101) plane [36]. The values tabulated in Table 2 indicate that the pure ZnO, ZnO-APTES, ZnO-PEG, ZnO-PVA and ZnO-PVP samples have crystallite size of 28.42 nm, 22.39 nm, 24.97 nm, 50.71 nm and 46.22 nm, respectively.

3.2. FESEM imaging

The morphology and microstructures of the prepared nanoparticle samples were characterized using a variable pressure field emission scanning electron microscope (FESEM, Zeiss Supra 55VP, Carl Zeiss) at an acceleration voltage of 5 kV and a magnification of 50,000. Histogram graphs were plotted with the aid of a Java-based image processing called ImageJ software to obtain the mean and standard deviation values from the particle size distributions. Since the expected nanoparticles shape is spherical, the size for all of the synthesized nanoparticles were measured by the diameter.

Based on Fig. 3, the average size obtained is at 24.41 nm + 5.5 7 nm. For the nanofluid formulation purpose, the small in size are much more preferable in order to ensure the stability of the nanoparticles in the base fluid. Hence, to synthesize TiO_2 nanoparticles, the optimum temperature and duration during the hydrothermal growth of the nanoparticles are at 120 °C for 12 h.

The size of the ZnO nanoparticles from Fig. 4 is ranged at 51.6 3 nm + 13.46 nm. Hydrothermal method is the preferred technique for both nanoparticles as it gives effective morphological control, a high degree of uniformity and suitable for mass production [37]. In the pressurized autoclave vessel, the nanoparticles grow by nucleation and snowballed into coagulation of particles with maintained temperature. Crystallization is influenced by induction, nucleation and growing processes. During induction, particles of critical size are produced. Next, critical-sized particles evolve into crystal cores

Table 2Calculated XRD characteristics for non-modified and modified ZnO.

Nanoparticle	FWHM (rad)	2θ (°)	D (nm)
ZnO	0.30733	36.28970	28.42
ZnO-APTES	0.39003	36.21091	22.39
ZnO-PEG	0.34983	36.23717	24.97
ZnO-PVA	0.17224	36.26343	50.71
ZnO-PVP	0.18906	36.42100	46.22

during nucleation. And further, solute molecules are arranged on the surface of existing nuclei and continue growing the crystals, as the pressure in the reactor increases when temperature increases [38].

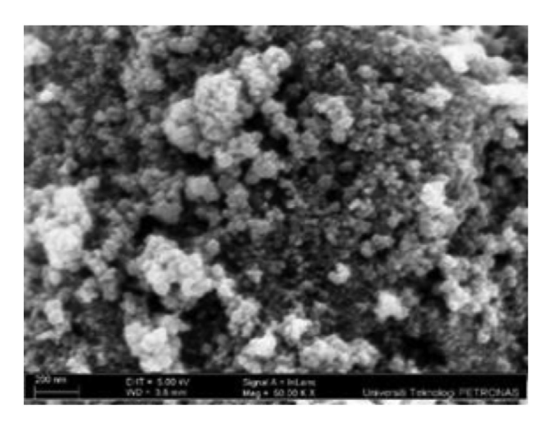
3.3. FTIR results

The functional groups of the amino silane and polymers in the nanoparticles were analyzed by Fourier Transform Infrared (FTIR) equipment, Perkin Elmer model. From the FTIR analysis, the transmittance of light at specific wavelengths is measured. The characteristics of the peaks recorded are classified into the type of peaks, chemical bonds and functional groups present.

Fig. 5 depicts FTIR spectra for pre- and post-functionalization of TiO_2 nanoparticles. The curves at 460–490 cm-1, 670–690 cm⁻¹ and 3440-3450 cm⁻¹ ranges showed the anatase characteristics from Ti-O, Ti-O-Ti and O-H respectively. The fingerprint region for pre-functionalized TiO2 differs from the post-functionalized signifying chemical interaction of TiO₂ with the amino silane and polymers. The increase in the intensity of Si-O-Si is observed at 1135 cm⁻¹ and 1000 cm⁻¹ because of amino-silane functional groups. The peaks at 1306 and 1494 cm⁻¹ indicate the presence of the NH₂ group and N—H bending, respectively. The small peak at 1648 cm⁻¹ corresponds to the stretching vibration of the C=N bond. The changes in the fingerprint region at 1656 cm⁻¹ due to C=O carbonyl stretch is believed to be due to PVA functionalization. The characteristic absorption peaks at 1135, 1453 and 836 cm⁻¹ represent the shoulder stretching of C—O, C—H bending and C-C stretching respectively. Further, the characteristic of C-O-C linkage is shown because of the presence of PEG. The vibration at 1626 cm⁻¹ corresponds to C=C bond stretching vibration for the modification by PEG [39]. The structural changes of TiO₂ due to interaction with PVP is indicated at 1650–1660 cm⁻¹ range from the presence of carbonyl group. C-H2 wagging and C-H stretching also can be seen at 1295 and 1462 cm⁻¹ respectively [40].

The % transmission of unmodified ZnO and functionalized ZnO by FTIR spectra are shown in Fig. 6. From spectra of modified ZnO and unmodified ZnO, the peaks for Zn-O were shown. As shown in the graph, the peak attributed to 1341 cm⁻¹ represents the N-O₃ bonding in ZnO [41].

For all of the samples, ZnO maximum is seen split into two maxima; one at 420-460 cm⁻¹ range and the other one is at 550-580 cm⁻¹ range [42]. Peaks at the 690 to 710 cm⁻¹ range represent the presence of Zn-O-Zn in all the samples [43]. The stretching vibration of absorbed water, as well as surface hydroxyl groups O—H were present in all curves, have been confirmed by the broad absorption band at 3200 to 3400 cm⁻¹ range. The peaks formed at about 1400 to 1500 cm⁻¹ are due to presence of H₂O on the molecules. Stretching of C—N is shown at the 1040 to 1060 cm⁻¹ range for ZnO and ZnO with polymers modification nanoparticles [44]. C=C stretching also can be seen at 1560 cm⁻¹ peak for ZnO and ZnO-APTES nanoparticles [45]. All of the modified ZnO with polymers showed C—H stretching at 1370 to 1400 cm⁻¹ range peak. The peak corresponding to the Si-O bond is observed at 993 cm⁻¹ and the N-H bending vibration was observed at 1666 cm⁻¹ which obtained from the amino silane in APTES. The characteristic peaks at 2943 and 736 cm⁻¹ attributed to C-H stretching and Si-O-C group [46]. The double bond of C=C also shown at 1560 cm⁻¹ due to APTES presence on the ZnO nanoparticles. As shown in Fig. 6, C-H₂ and C—O stretching vibrations can be seen at 2936 and 1102 cm⁻¹, which demonstrated the presence of PVA onto the ZnO particle surface [47]. The appearance of N—H linkage at 1557 cm⁻¹ indicates the presence of PEG polymer in the ZnO-PEG [48]. Next, the presence of the carbonyl group is



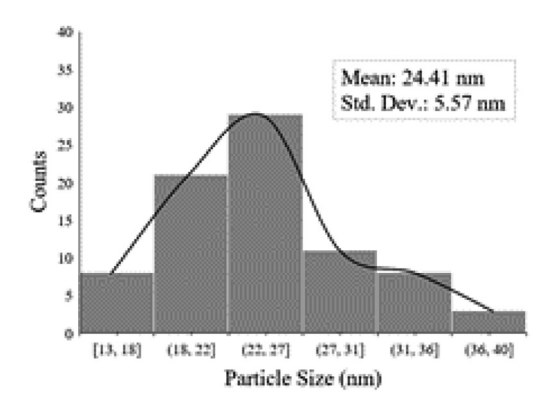
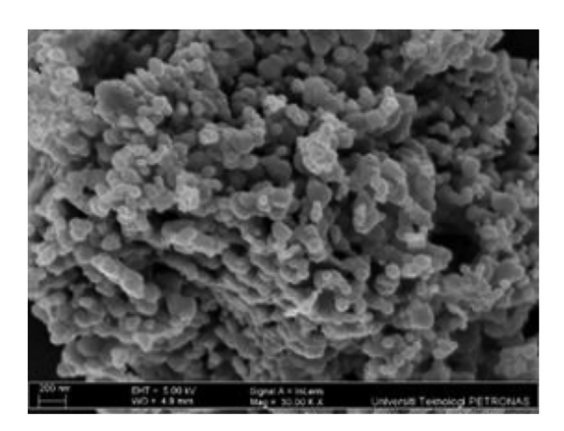


Fig. 3. FESEM image and particle size distribution histogram for non-modified TiO₂ nanoparticles.



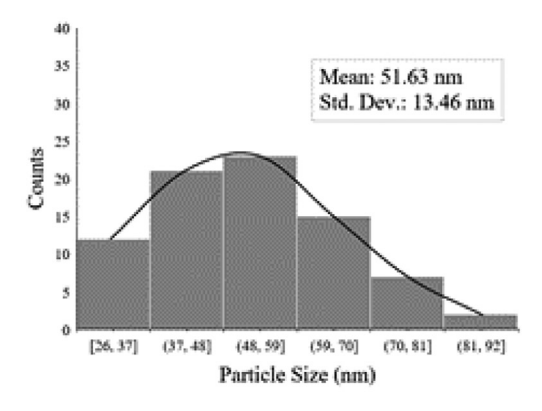


Fig. 4. FESEM image with particle size distribution histogram for non-modified ZnO nanoparticles.

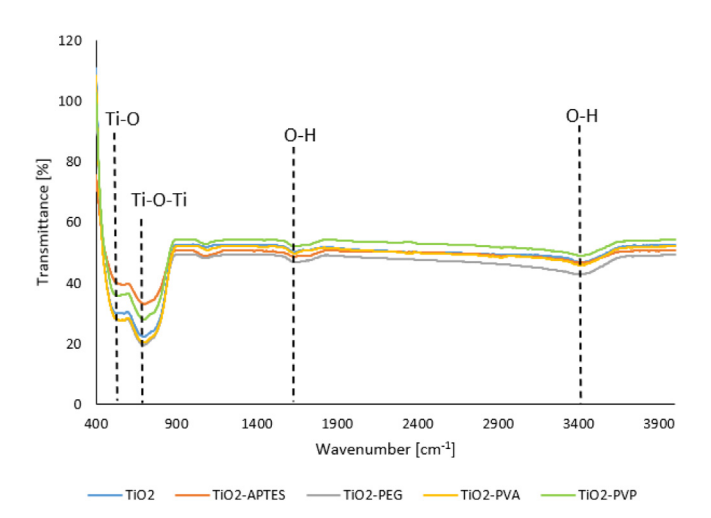


Fig. 5. FTIR graph on TiO_2 and surface-modified TiO_2 nanoparticles.

shown at 1650 to 1660 $\rm cm^{-1}$ range due to the functionalization of PVP.

3.4. TEM analysis

The TEM modelled Zeiss Libra 200FE was performed at an acceleration voltage of 120 kV and a magnification of 800,000 for the surface modified TiO₂ nanoparticles. Meanwhile, for surface modified ZnO nanoparticles, the TEM analysis was done at an acceleration voltage of 120 kV and a magnification of 200,000. The analysis

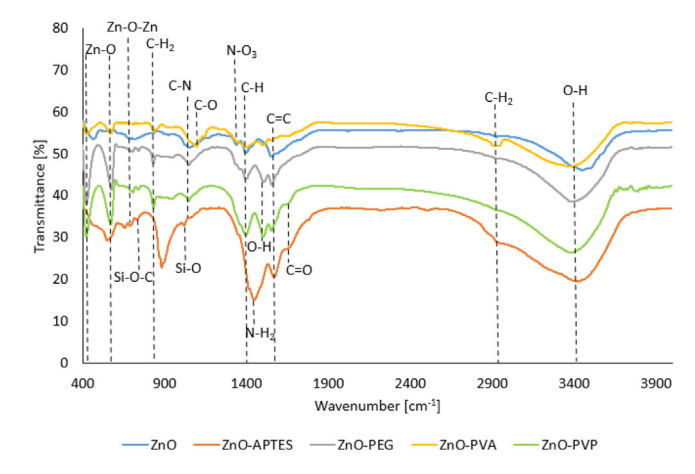


Fig. 6. FTIR graph on ZnO and surface-modified ZnO nanoparticles.

done for surface modified ZnO samples used lower magnification as compared to the surface modified ${\rm TiO_2}$ samples because the particle size of surface modified ZnO samples is higher than that of ${\rm TiO_2}$. Coating thickness histograms were plotted as the measurements made from the TEM images were done by ImageJ software.

The coating of APTES, PEG, PVA and PVP on the surface of TiO_2 nanoparticles are shown in Fig. 7 together with the coating thickness histograms. The methodology and concentration applied for the coating of the amino silane and polymers on the surface of TiO_2 nanoparticles were the same. From the histograms constructed, the coating thickness for all types of samples was uni-

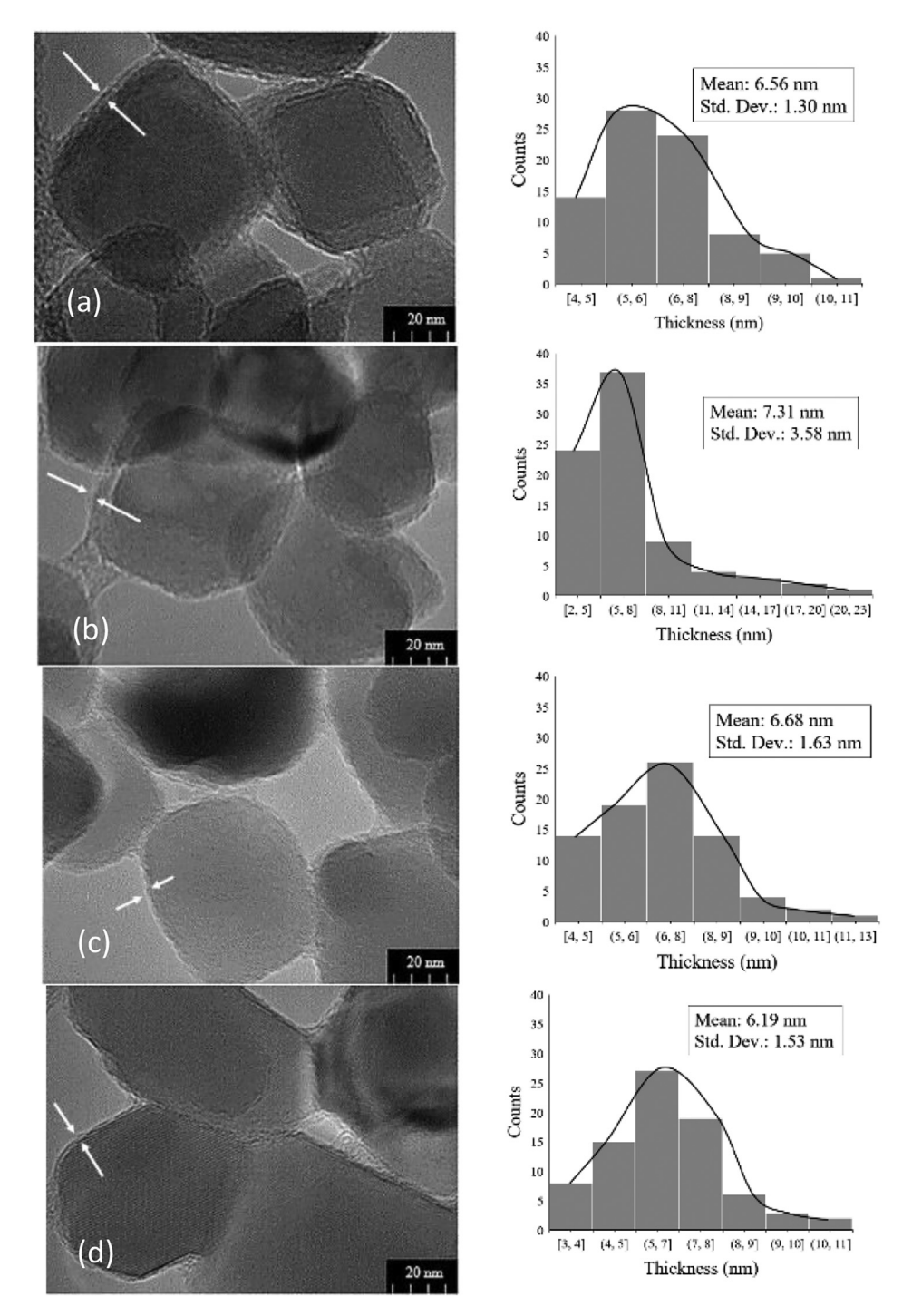


Fig. 7. TEM images and coating thickness histograms for (a) TiO₂-APTES nanoparticles, (b) TiO₂-PEG nanoparticles, (c) TiO₂-PVA nanoparticles and (d) TiO₂-PVP nanoparticles.

form. The average coating thickness for the synthesized modified TiO_2 nanoparticles are 6.56 nm \pm 1.30 nm, 7.31 nm \pm 3.58 nm, 6. 68 nm \pm 1.63 nm and 6.19 nm \pm 1.53 nm for TiO_2 -APTES, TiO_2 -PEG, TiO_2 -PVA and TiO_2 -PVP, respectively.

The measurement of the TEM images was done using a Javabased image processing program which is ImageJ software. The radius of the nanoparticles for each sample was also measured and the values obtained are 118.35 nm \pm 13.30 nm, 110.44 nm \pm 4. 91 nm, 100.46 nm \pm 6.41 nm and 93.08 nm \pm 11.73 nm for TiO₂-APTES, TiO₂-PEG, TiO₂-PVA and TiO₂-PVP, respectively. The size of the modified nanoparticles is increasing in size due to the coating effect.

The purpose of the coating is to enhance the stability of ${\rm TiO_2}$ nanoparticles in the base fluid by increasing the repulsive forces between each particle. The repulsion can be induced sterically due to the coating on the nanoparticles surface. The molecules from the amino-silane and the polymers provide steric hindrance on the surface of nanoparticles. Therefore, the compatibility between the nanoparticles and the amino silane and polymers applied is crucial for the stability of nanofluids produced.

From Fig. 8, the coating of PEG and PVA on the ZnO nanoparticles can be seen clearly in the images. Meanwhile, surface modification by using APTES and PVP did not give the expected

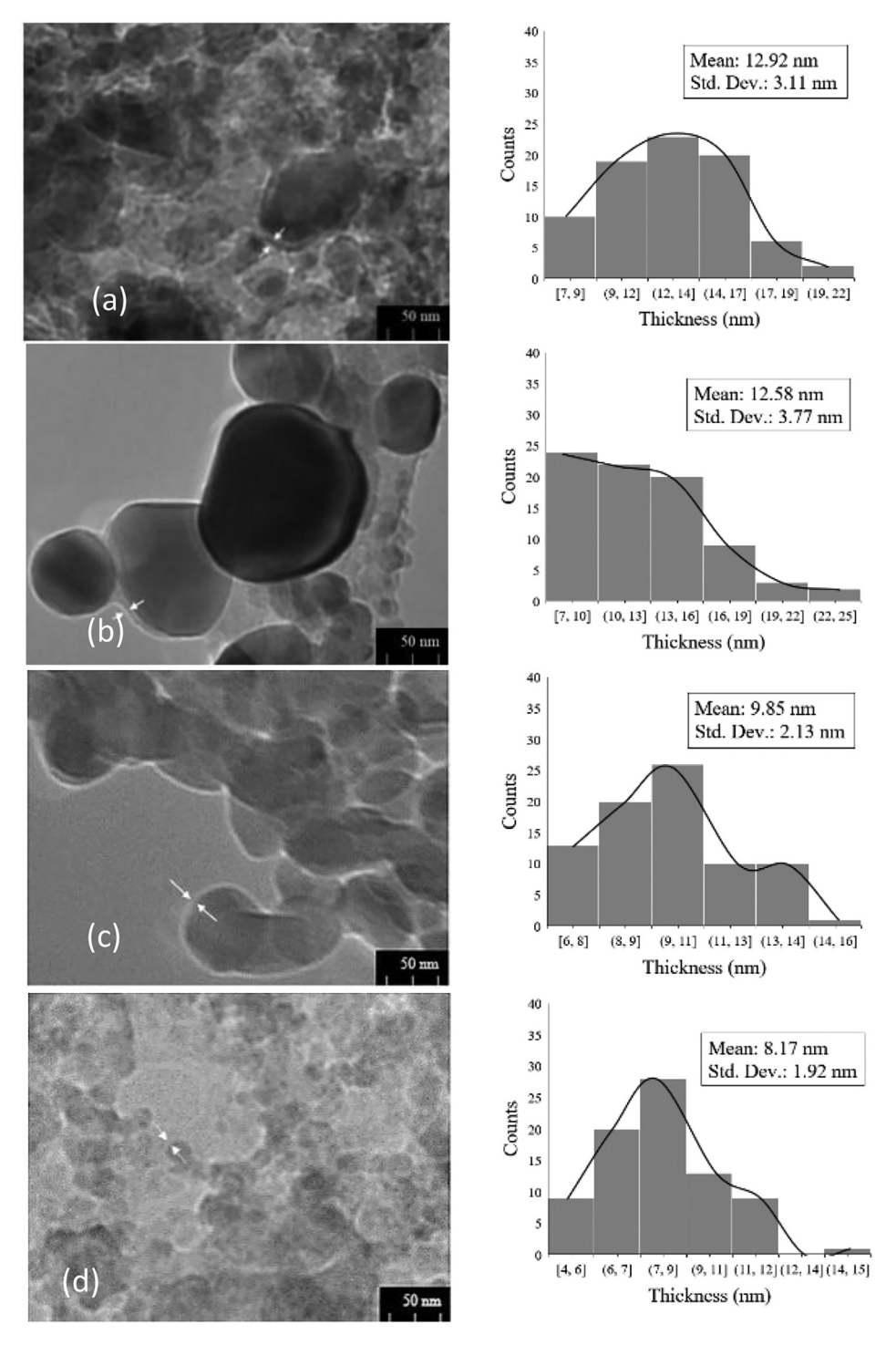


Fig. 8. TEM images and coating thickness histograms for (a) ZnO-APTES nanoparticles, (b) ZnO-PEG, (c) ZnO-PVA and (d) ZnO-PVP nanoparticles.

outcome of increase the repulsive force between the particles to each other.

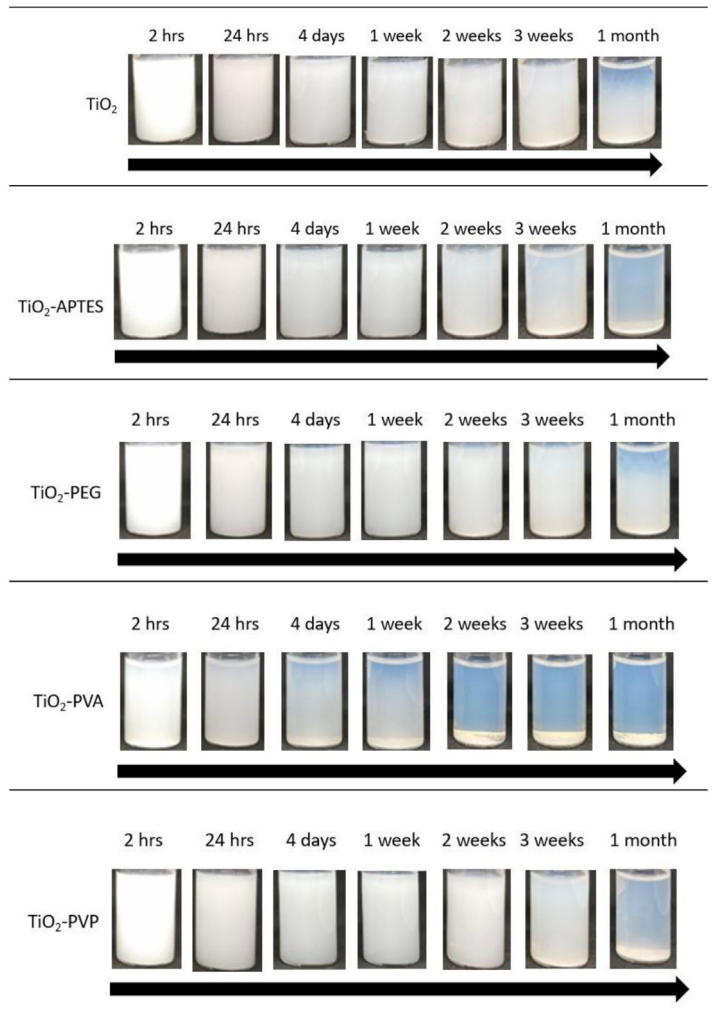
As seen from the figure, the histograms constructed give the average coating thickness for each sample. The values obtained are 12. 92 nm \pm 3.11 nm, 12.58 nm \pm 3.77 nm, 9.85 nm \pm 2.13 nm and 8.17 nm \pm 1.92 nm for ZnO-APTES, ZnO-PEG, ZnO-PVA and ZnO-PVP, respectively. The measurements made from the TEM images were done by ImageJ software. Besides, the radius of each particle is measured to be about 81.14 nm \pm 36.92, 115.74 nm \pm +10.88 nm, 71.90 nm \pm 10.93 nm and 81.02 nm \pm 38.29 nm, respectively.

3.5. Nanofluids stability

The optical images of the dispersion of the unmodified and modified TiO_2 nanoparticles in the base fluid are shown in Table 2. The TiO_2 -PVA suspension shows the quickest separation time forming sediments and a clear supernatant on the top. The separation interfaces between the sediment and the supernatant were sharp and moved downward with time.

After a week, the unmodified TiO₂ shows that the sedimentations have been accumulated at the bottom with the column of

Table 3 Physical observation on unmodified and modified TiO_2 nanofluids in a month.



cloudy supernatant suspensions have settled. Meanwhile, TiO_2 -PEG, TiO_2 -APTES and TiO_2 -PVP nanoparticles-based nanofluids are started to accumulate at the bottom of the vials, yet there is no visible phase separation exist. After two weeks, both unmodified TiO_2 and TiO_2 -PVA have shown two-phase separation with sediment layer at the bottom of the vials with clear liquid at the top.

Based on the observation made, it can be deduced that TiO₂-PEG, TiO₂-APTES and TiO₂-PVP nanoparticles-based nanofluids showed good dispersion for over 7 days. From merely physical observation, the typical behavior of a well-dispersed solution is difficult to confirm. Hence, the stability of the nanofluids need to be analyzed by the zeta potential analyzer for more accurate readings.

The stability of the unmodified and modified ZnO nanofluids are shown in Table 3. The ZnO-APTES suspension is seen to be separated very quickly into sediments and a clear supernatant on top of the sediment. The separation interfaces between the sediment and the supernatant are sharp and moved downward with time. At day 1, sedimentations can be seen accumulated at the bottom of the vial for the unmodified ZnO nanofluid, as the suspension is cloudy, but the nanoparticles are starting to settle at the bottom. However, good dispersion can still be seen for both ZnO-PEG and ZnO-PVP nanofluids.

After a month, all three of the unmodified ZnO, ZnO-APTES and ZnO-PVP showed distinct phase separations between the agglom-

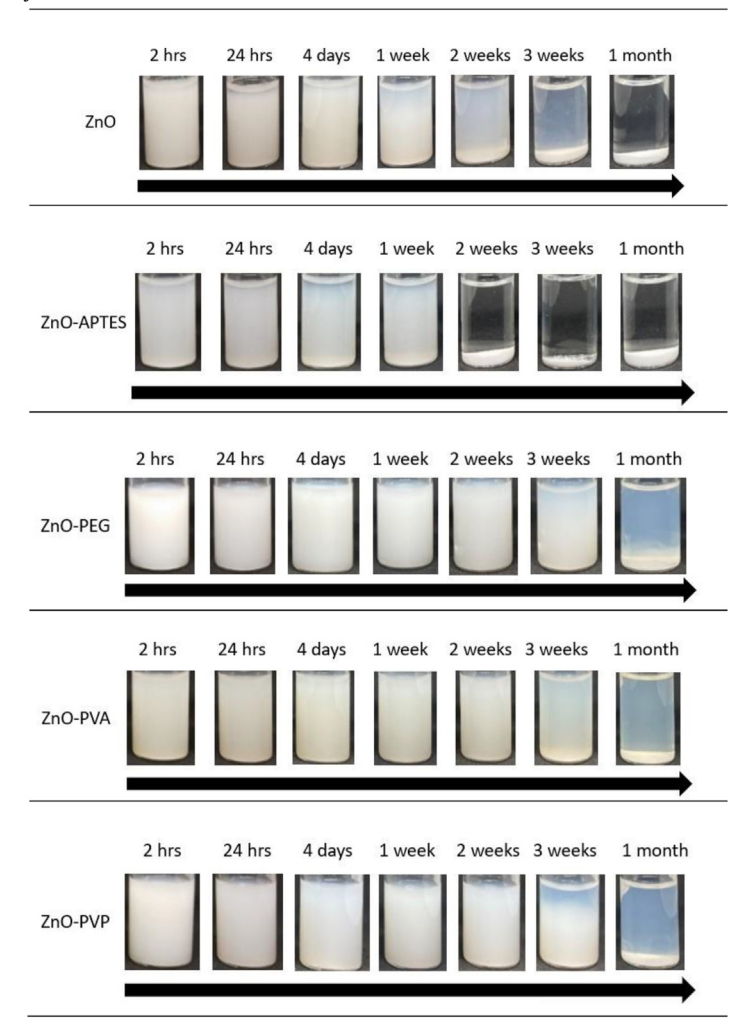
erated sediments with the clear base fluid. On the other hand, the suspension for ZnO-PEG and ZnO-PVA still showing the typical behavior of a well-dispersed solution at 1-month period of time. To indicate the surface modification from polymer that leads to increased stability of ZnO nanoparticles, zeta potential analysis needs to be done.

The stability of nanoparticles in base fluids was verified by zeta potential analysis. The stability of nanofluids with different chemicals used for surface modification was compared. Zeta potential analysis was conducted on nanofluids at 0.25 wt% concentration in 10 ml of 0.002 molL⁻¹ brine solution. A reliable zeta potential value to confirm the stability and dispersion of nanoparticles in base fluids is above 30 mV [49].

Particle size analysis was carried out using Malvern Master Sizer 2000 where it is used to measure the particle size where the scattered light intensity from the passing laser beam through the dispersed particulate sample is measured. According to Malvern's manual, the equipment determines the electrophoretic mobility and convert to zeta potential by applying Henry equation as shown in Equation (2). Electrophoretic mobility is measured as the system is put in a cell with electrodes and particles move towards the electrode of opposite charge. The velocity of the particles is measured and expressed as mobility.

$$U_E = \frac{2\varepsilon \zeta f(\kappa \alpha)}{3\eta} \tag{2}$$

Table 4Physical observation on unmodified and modified ZnO nanofluids in a month.



From the equation, ζ is zeta potential, U_E is electrophoretic mobility, ϵ is dielectric constant, η is viscosity and $f(\kappa\alpha)$ is Henry's function. The value for $f(\kappa\alpha)$ is 1.5 as referred to Smoluchowski approximation.

Table 4 displayed the values obtained for both non-modified and modified TiO₂ and ZnO nanofluids. The highest zeta potential values obtained for the TiO₂-based is TiO₂-PVP and for the ZnO-based is ZnO-PEG. Meanwhile, the least values obtained are TiO₂-PVA and ZnO-APTES.

As compared to previous reports, there is a study on $CoFe_2O_4$ functionalized with N-(2-Amino-ethyl) 3-aminopropyl trimethoxy-silane with 0.005 wt% concentration in deionized water at pH 11 and obtained the zeta potential value at 30.0 mV [50]. Another formulated $CoFe_2O_4$ functionalized with aminodextran (AMD) nanofluid has obtained stability at 38.0 mV as the zeta potential result when the concentration of nanoparticles applied was at 0.02 wt% in deionized water with alkalinity at pH 11 [51]. Further, a formulated SiO_2 -APTES resulted with 40.0 mV zeta

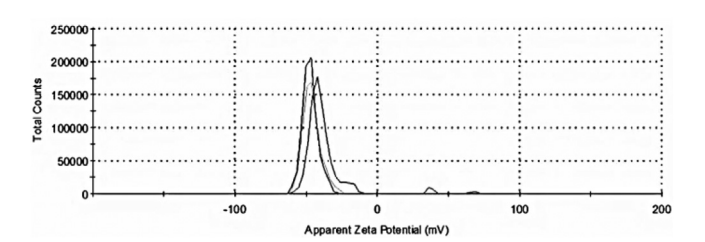


Fig. 9. Zeta potential distribution graph for TiO₂-PVP nanofluids.

potential value when the conducted study was done at 0.1 wt% in deionized water at pH 9 [52]. Next, the stability of both FeS nanofluid with neutral pH [53] and 1,3,5-trinitroperhydro-1,3,5-triazine (RDX) nanofluid with weight percent at 0.1 and alkali environment at pH 11 [54] obtained zeta potential values less than 30.0 mV. Nanofluids stability done by previous studies have been formulated using different parameters but with one common vari-

Table 5Zeta potential values for non-modified and modified TiO₂ and ZnO nanofluids.

Sample	Non-modified	-APTES	-PEG	-PVA	-PVP
TiO ₂	3.3 mV	25.2 mV	40.3 mV	2.3 mV	47.2 mV
ZnO	30.7 mV	13.9 mV	56.5 mV	48.7 mV	39.6 mV

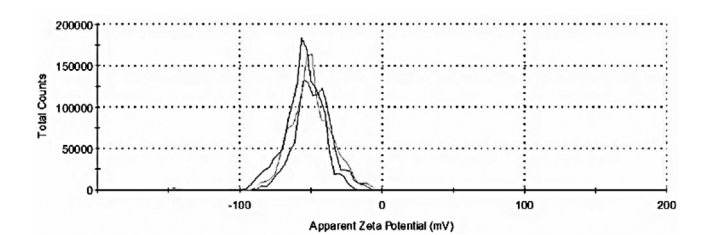


Fig. 10. Zeta potential distribution graph for ZnO-PEG nanofluids.

able to the least which is formulation of nanofluids using surface-modified or functionalized nanoparticles. Through this research work, nanofluids formulated using surface-modified ${\rm TiO_2}$ and ZnO nanoparticles by the previously mentioned synthesis and preparation methods managed to obtain stable zeta potential values stability for over 2 weeks as seen in Table 5, hence, made the findings from this study to further contribute and expand the horizon of this field of study.

Fig. 9 and Fig. 10 show the graphs attained based on the most stable nanofluids from surface modified TiO₂ and ZnO nanofluid samples. The measurements were taken at 0.25 wt% surface modified nanoparticles concentration in 10 ml of 0.002 molL⁻¹ brine solution with alkalinity at pH 10.

From the values obtained, it can be deduced that PVP functionalization can enhance the stability of TiO₂ nanoparticles whilst PEG is the best functionalization to improve the stability of ZnO-based nanofluid. The amino silane coating by APTES suppressed the dispersion of ZnO nanofluid. Upon the amino functionalization of the ZnO nanoparticles, the stability of the dispersions did not improve due to the hydrophobic interactions between nanoparticles [55].

The addition of amino silane increases the molecular weight of the synthesized nanoparticles, results in a stronger dispersion force since the particle eventually become larger and heavier with the presence of the amino silane. On the other hand, the coating by PVA polymer on TiO₂ nanoparticles give the least value of zeta potential as the adhesion of the polymer on the surface of the synthesized nanoparticles causes the charge to facilitate the adsorption of the polymer. The zeta potential values obtained for other nanofluids above 30 mV is considered as moderate or in the range of good stability [42]. In other words, low-value zeta potential indicates that the particles are agglomerated among another. Due to the high surface-to-volume ratio, nanoparticles are prone to be attacked by oxidative or corrosive environments that can change their structural properties. Hence, surface modification by coatings and functionalization improves the dispersion stability.

4. Conclusion

This report contributes in the field of nanofluids as the modus operandi in formulating stable and longer agglomeration rate is comprehensively presented stepwise. Obtaining a stable nanofluid with respect to compatible polymer is very important prior to application in any fields or systems. Consumption of resources and time can be reduced significantly if the preparation and synthesis process of the nanoparticles and nanofluids is designed with precision. From the experimental work, it is found that $\rm TiO_2\text{-PVP}$ and $\rm ZnO\text{-PEG}$ are the compatible polymer coating nanoparticles. The blended nanocomposites are synthesized by hydrothermal method at 120 °C for 12 h and at 100 °C for 2 h respectively. The synthesis and preparation methods with polymeric surface modification alternative for the nanofluid stability enhancement resulted zeta potential values at 47.2 mV and 56.5 mV for both of the men-

tioned nanofluids accordingly with agglomeration rate up to two weeks.

Ethical statement

This paper is the authors' own original work, which has not been previously published elsewhere, not currently being considered for publication elsewhere and reflects the authors' own research and analysis in a truthful and complete manner.

Funding

This research was funded by International Grant Universitas Islam Riau-Universiti Teknologi PETRONAS (UIR-UTP) with cost center 015ME0-042.

Declaration of Competing Interest

The authors declare that they have no known competing financial interests or personal relationships that could have appeared to influence the work reported in this paper.

Acknowledgments

The authors would like to acknowledge UTP Graduate Assistantship (GA) scheme, International Grant UIR-UTP 015ME0-042 and Department of Fundamental and Applied Sciences, Universiti Teknologi PETRONAS for their support in the research work.

References

- [1] N. Ali, J.A. Teixeira, A. Addali, A review on nanofluids: fabrication, stability, and thermophysical properties, J. Nanomater. 2018 (2018) 1–33.
- [2] S.K. Choi, H.A. Son, H.T. Kim, J.W. Kim, Nanofluid enhanced oil recovery using hydrophobically associative zwitterionic polymer-coated silica nanoparticles, Energy Fuel 31 (8) (2017) 7777–7782, https://doi.org/10.1021/acs. energyfuels.7b00455.
- [3] A. Sircar, K. Rayavarapu, N. Bist, K. Yadav, S. Singh, Applications of nanoparticles in enhanced oil recovery, Petroleum Res. 7 (1) (2022) 77–90.
- [4] X. Sun, Y. Zhang, G. Chen, Z. Gai, Application of nanoparticles in enhanced oil recovery: a critical review of recent progress, Energies 10 (3) (2017) 345, https://doi.org/10.3390/en10030345.
- [5] V. Barkhordari, A. Jafari, Experimental investigation of the base fluid miscibility condition on the oil recovery using nanofluids flooding, J. Water Environ. Nanotechnol. 3 (1) (2018) 12–21, https://doi.org/10.22090/jwent.2018.01.002.
- [6] C. Anushree, J. Philip, Assessment of long-term stability of aqueous nanofluids using different experimental techniques, J. Mol. Liq. 222 (2016) 350–358, https://doi.org/10.1016/j.molliq.2016.07.051.
- [7] M.T. Ramesan, K.P. Greeshma, K. Parvathi, T. Anilkumar, Structural, electrical, thermal, and gas sensing properties of new conductive blend nanocomposites based on polypyrrole/phenothiazine/silver-doped zinc oxide, J Vinyl Addit Technol 26 (2020) 187–195, https://doi.org/10.1002/vnl.21732.
- [8] K. Suhailath, M.T. Ramesan, Effect of nano-Ce-doped TiO2 on AC conductivity and DC conductivity modeling studies of poly (n-butyl methacrylate), J. Electron. Mater 47 (2018) 6484–6493, https://doi.org/10.1007/s11664-018-6556-3.
- [9] K. Li, D. Wang, S. Jiang, Review on enhanced oil recovery by nanofluids, Oil Gas Sci. Technol. 73 (2018) 37, https://doi.org/10.2516/ogst/2018025.
- [10] A.R. Ismail, A. Aftab, Z.H. Ibupoto, N. Zolkifile, The novel approach for the enhancement of rheological properties of water-based drilling fluids by using multi-walled carbon nanotube, nanosilica and glass beads, J. Pet. Sci. Eng. 139 (2016) 264–275, https://doi.org/10.1016/j.petrol.2016.01.036.
- [11] K. Karakosta, A.C. Mitropoulos, G.Z. Kyzas, A review in nanopolymers for drilling fluids applications, J. Mol. Struct. 129702 (2020) 1–8, https://doi.org/ 10.1016/j.molstruc.2020.129702.
- [12] A. Aftab, A.R. Ismail, Z.H. Ibupoto, H. Akeiber, M.G.K. Malghani, Nanoparticles based drilling muds a solution to drill elevated temperature wells: A review, Renew. Sustain. Energy Rev. 76 (2017) 1301–1313, https://doi.org/10.1016/j. rser.2017.03.050.
- [13] M.I. Abduo, A.S. Dahab, H. Abuseda, A.M. Abdul Aziz, M.S. Elhossieny, Comparative study of using water-based mud containing multiwall carbon nanotubes versus oil-based mud in HPHT fields, Egypt. J. Petrol 25 (4) (2016) 459–464, https://doi.org/10.1016/j.ejpe.2015.10.008.
- [14] S.U. Ilyas, R. Pendyala, N. Marneni, Stability of nanofluids, Topics Mining, Metallurgy Mater. Eng. 1–31 (2017), https://doi.org/10.1007/978-3-319-29761-3_1.

- [15] K. Suhailath, M.T. Ramesan, Investigations on the structural, mechanical, thermal, and electrical properties of Ce-doped TiO₂/poly(n-butyl methacrylate) nanocomposites, J. Therm. Anal. Calorim. 135 (2019) 2159–2169, https://doi.org/10.1007/s10973-018-7285-9.
- [16] M. Goodarzi, D. Toghraie, M. Reiszadeh, M. Afrand, Experimental evaluation of dynamic viscosity of ZnO–MWCNTs/engine oil hybrid nanolubricant based on changes in temperature and concentration, J. Therm. Anal. Calorim. 136 (2019) 513–525, https://doi.org/10.1007/s10973-018-7707-8.
- [17] Z.X. Li, F.L. Renault, A.O.C. Gómez, M.M. Sarafraz, H. Khan, M.R. Safaei, F.E. Bandarra, Nanofluids as secondary fluid in the refrigeration system: experimental data, regression, ANFIS, and NN modeling, Int. J. Heat Mass Transf. 144 (2019), https://doi.org/10.1016/j.ijheatmasstransfer.2019.118635.
- [18] Safaei, M. R., Jahanbin, A., Kianifar, A., Gharehkhani, S., Kherbeet, A. S., and Dahari, M. G. M. (2016). Mathematical Modeling for Nanofluids Simulation: A Review of the Latest Works. In N. S. Akbar, & O. A. Beg (Eds.), Modeling and Simulation in Engineering Sciences. *IntechOpen*. https://doi.org/10.5772/ 64154.
- [19] Liu, W., Malekahmadi, O., Bagherzadeh, A., Ghashang, M., Hasani, S., Tlili, I. and Goodarzi, M. (2019). A novel comprehensive experimental study concerned graphene oxide nanoparticles dispersed in water: Synthesise, characterisation, thermal conductivity measurement and present a new approach of RLSF neural network. *Int. Commun. Heat Mass Transfer*, 109, 104333. https://doi.org/ 10.1016/j.icheatmasstransfer.2019.104333.
- [20] M. Afrand, K. Nazari Najafabadi, N. Sina, M.R. Safaei, A.S. Kherbeet, S. Wongwises, M. Dahari, Prediction of dynamic viscosity of a hybrid nanolubricant by an optimal artificial neural network, Int. Commun. Heat Mass Transfer 76 (2016) 209–214.
- [21] K. Bashirnezhad, S. Bazri, M.R. Safaei, M. Goodarzi, M. Dahari, O. Mahian, A. S. Dalkılıça, S. Wongwises, Viscosity of nanofluids: a review of recent experimental studies, Int. Commun. Heat Mass Transfer 73 (2016) 114-123
- [22] M.S. Kamal, A.A. Adewunmi, A.S. Sultan, M.F. Al-Hamad, U. Mehmood, Recent advances in nanoparticles enhanced oil recovery: rheology, interfacial tension, oil recovery, and wettability alteration, J. Nanomater. 2017 (2017) 1–15, https://doi.org/10.1155/2017/2473175.
- [23] L.M. Corredor-Rojas, A. Hemmati-Sarapardeh, M.M. Husein, M. Dong, B.B. Maini, Rheological behavior of surface modified silica nanoparticles dispersed in Partially Hydrolyzed Polyacrylamide and Xanthan Gum solutions: experimental measurements, mechanistic understanding, and model development, Energy Fuel 32 (10) (2018) 10628-10638.
- [24] A. Banerjee, S.K. Ray, Synthesis of chitosan grafted polymethyl methacrylate nanopolymers and its effect on polyvinyl chloride membrane for acetone recovery by pervaporation, Carbohydr. Polym. 258 (2021), https://doi.org/ 10.1016/j.carbpol.2021.117704 117704.
- [25] M. Ali, H.H. Jarni, A. Aftab, A.R. Ismail, N.M.C. Saady, M.F. Sahito, A. Keshavarz, S. Iglauer, M. Sarmadivaleh, Nanomaterial-based drilling fluids for exploitation of unconventional reservoirs: a review, Energies 13 (13) (2020) 3417, https:// doi.org/10.3390/en13133417.
- [26] Z. Zhe, A. Yuxiu, Nanotechnology for the oil and gas industry an overview of recent progress, Nanotechnol. Rev. 7 (4) (2018) 341–353, https://doi.org/ 10.1515/ntrev-2018-0061.
- [27] N.A. Alshehri, A.R. Lewis, C. Pleydell-Pearce, T.G.G. Maffeis, Investigation of the growth parameters of hydrothermal ZnO nanowires for scale up applications, J. Saudi Chem. Soc. 22 (5) (2018) 538–545, https://doi.org/10.1016/j. iscs.2017.09.004.
- [28] H.S. Wasly, M.S.A. El-Sadek, M. Henini, Influence of reaction time and synthesis temperature on the physical properties of ZnO nanoparticles synthesized by the hydrothermal method, Appl. Phys. A 124 (1) (2018) 1–12, https://doi.org/ 10.1007/s00339-017-1482-4.
- [29] Bahrani, S., Ghaedi, M., Tariq, R., Zalipour, Z. and Sadeghfar, F. (2021). Chapter 8 Fundamental developments in the zeolite process. *Interface Sci. Technol.*, 32 (2021), 499–556. http://dx.doi.org/10.1016/B978-0-12-818806-4.00003-6.
- [30] T. Wirunmongkol, N. O-Charoen, S. Pavasupree, Simple hydrothermal preparation of zinc oxide powders using Thai autoclave unit, Energy Procedia 34 (2013) 801–807.
- Procedia 34 (2013) 801–807.

 [31] S. Mohan, M. Vellakkat, A. Aravind, Hydrothermal synthesis and characterization of Zinc Oxide nanoparticles of various shapes under different reaction conditions, Nano Express 1 (3) (2020) 1–15, https://doi.org/10.1088/2632-959X/abc813.
- [32] P.M. Aneesh, K.A. Vanaja, M.K. Jayaraj, Synthesis of ZnO nanoparticles by hydrothermal method, Nanophotonic Mater. IV 1–9 (2007), https://doi.org/ 10.1117/12.730364.
- [33] Klaysri, R., Tubchareon, T., and Praserthdam, P. (2017). One-step synthesis of amine-functionalized TiO₂ surface for photocatalytic decolorization under visible light irradiation. J. Ind. Eng. Chem., 45, 229-236. http://dx.doi.org/ 10.1016%2Fj.jiec.2016.09.027.

- [34] J. Kapica-Kozar, E. Piróg, E. Kusiak-Nejman, R.J. Wrobel, A. Gęsikiewicz-Puchalska, A.W. Morawski, U. Narkiewiez, B. Michalkiewicz, Titanium dioxide modified with various amines used as sorbents of carbon dioxide, New J. Chem. 41 (4) (2017) 1549–1557, https://doi.org/10.1039/C6NJ02808J.
- [35] R. Khan, S. Javed, M. Islam, Hierarchical nanostructures of titanium dioxide: synthesis and applications, Titanium Dioxide – Mater. Sustainable Environ. 1 (2018) 1–38, https://doi.org/10.5772/intechopen.74525.
- [36] J.N. Hasnidawani, H.N. Azlina, H. Noritan, N. Bonnia, S. Ratim, E.S. Ali, Synthesis of ZnO nanostructures using sol-gel method, Procedia Chem. 19 (2016) 211– 216, https://doi.org/10.1016/J.PROCHE.2016.03.095.
- [37] F. Wang, L. Zhu, Q. Wei, Y. Wang, Research on the effects of hydrothermal synthesis conditions on the crystal habit of MIL-121, R. Soc. Open Sci. 7 (201212) (2020) 1–11, https://doi.org/10.1098/rsos.201212.
- [38] N. Deilami, A. Haghighatzadeh, Investigating the effects of hydrothermal temperature on morphology-controlled synthesis of flower-shaped ZnO microstructures, J. Aust. Ceram. Soc. 57 (2) (2021) 409–418, https://doi.org/ 10.1007/s41779-020-00553-2.
- [39] A. León, P. Reuquen, C. Garín, R. Segura, P. Vargas, P. Zapata, P.A. Orihuela, FTIR and Raman characterization of TiO₂ nanoparticles coated with polyethylene glycol as carrier for 2-methoxyestradiol, Appl. Sci. 7 (1) (2017) 49, https://doi. org/10.3390/app7010049.
- [40] P. Pandey, M. Dahiya, A brief review on inorganic nanoparticles, J. Critical Rev. 3 (3) (2016) 18–26.
- [41] K. Rokesh, A. Nithya, K. Jeganathan, K. Jothivenkatachalam, A facile solid-state synthesis of cone-like ZnO microstructure an efficient solar-light driven photocatalyst for rhodamine B degradation, Mater. Today:. Proc. 3 (2016) 4163–4172, https://doi.org/10.1016/j.matpr.2016.11.091.
- [42] K. Lefatshe, C.M. Muiva, L.P. Kebaabetswe, Extraction of nanocellulose and insitu casting of ZnO/cellulose nanocomposite with enhanced photocatalytic and antibacterial activity, Carbohydr. Polym. 164 (2017) 301–308, https://doi.org/10.1016/j.carbpol.2017.02.020.
- [43] R. Patiño-Herrera, R. Catarino-Centeno, M. Robles-Martínez, M.G.M. Zarate, J.-C. Flores-Arriaga, E. Pérez, Antimycotic activity of zinc oxide decorated with silver nanoparticles against Trichophyton mentagrophytes, Powder Technol. 327 (2018) 381–391, https://doi.org/10.1016/j.powtec.2018.01.004.
- [44] P. Nyamukamba, O. Okoh, H. Mungondori, R. Taziwa, S. Zinya, Synthetic methods for titanium dioxide nanoparticles: a review, Titanium Dioxide – Mater. Sustainable Environ. 8 (2018) 151–175, https://doi.org/10.5772/ intechopen.75425.
- [45] W. Muhammad, N. Ullah, M. Haroon, B.H. Abbasi, Optical, morphological and biological analysis of zinc oxide nanoparticles (ZnO NPs) using Papaver somniferum L, RSC Adv. 9 (2019) 29541–29548, https://doi.org/10.1039/ C9RA04424H.
- [46] S. Ramkissoon, D. Alexander, R. Maharaj, M. Soroush, Evaluation of a low salinity water fooding with polymer gel treatment in Trinidad and Tobago, J. Pet. Explor. Prod. Technol. 10 (2020) (2020) 3971–3981, https://doi.org/ 10.1007/s13202-020-00991-5.
- [47] I. Korbag, S. Mohamed Saleh, Studies on the formation of intermolecular interactions and structural characterization of polyvinyl alcohol/lignin film, Int. J. Environ. Stud. 73 (2) (2016) 226–235, https://doi.org/10.1080/ 00207233.2016.1143700.
- [48] H. Hayashi, Y. Hakuta, Hydrothermal synthesis of metal oxide nanoparticles in supercritical water, Materials 3 (7) (2010) 3794–3817.
- [49] M. Arulprakasajothi, K. Elangovan, U. Chandrasekhar, S. Suresh, Performance study of conical strip inserts in tube heat exchanger using water-based titanium oxide nanofluid, Therm. Sci. 22 (1) (2018) 477–485, https://doi.org/ 10.2298/TSC1151024250A.
- [50] S. Yavari, N.M. Mahmodi, P. Teymouri, B. Shahmoradi, A. Maleki, Cobalt ferrite nanoparticles: Preparation, characterization and anionic dye removal capability, J. Taiwan Inst. Chem. Eng. 59 (2016) 320–329.
 [51] S. Khizar, N.M. Ahmad, N. Ahmed, S. Manzoor, M.A. Hamayun, N. Naseer, M.K.L.
- [51] S. Khizar, N.M. Ahmad, N. Ahmed, S. Manzoor, M.A. Hamayun, N. Naseer, M.K.L. Tenorio, N. Lebaz, A. Elaissari, Aminodextran coated CoFe2O4 nanoparticles for combined magnetic resonance imaging and hyperthermia, Nanomaterials 10 (11) (2020) 2182–2198.
- [52] V. Fuskele, R.M. Sarviya, Recent developments in nanoparticles synthesis, preparation and stability of nanofluids, Mater. Today.. Proc. 4 (2017) 4049– 4060
- [53] S. Luo, X. Nie, M. Yang, Y. Fu, P. Zeng, Q. Wan, Sorption of differently charged gold nanoparticles on synthetic pyrite, Minerals 8 (10) (2018) 428–441.
- [54] M. Doukkali, R.B. Patel, V. Stepanov, H. Hadim, The effect of ionic strength and pH on the electrostatic stabilization of NanoRDX, Propellants Explos. Pyrotech. 42 (9) (2017) 1066–1071.
- [55] M.C. Ruiz-Cañas, L.M. Corredor, H.I. Quintero, E. Manrique, A.R.R. Bohórquez, Morphological and structural properties of amino-functionalized fumed nanosilica and its comparison with nanoparticles obtained by modified Stöber method, Molecules 25 (12) (2020) 2868–2885, https://doi.org/ 10.3390/molecules25122868.